J. Fluid Mech. (2007), *vol.* 583, *pp.* 1–26.
doi:10.1017/S0022112007005885 Printed in the United Kingdom

On transition to cellularity in expanding spherical flames

G. JOMAAS[1], C. K. LAW[1] AND J. K. BECHTOLD[2]

[1]Princeton University, Princeton, NJ 08544, USA

[2]New Jersey Institute of Technology, Newark, NJ 07102, USA

(Received 29 April 2006 and in revised form 7 January 2007)

The instant of transition to cellularity of centrally ignited, outwardly propagating spherical flames in a reactive environment of fuel–oxidizer mixture, at atmospheric and elevated pressures, was experimentally determined using high-speed schlieren imaging and subsequently interpreted on the basis of hydrodynamic and diffusional–thermal instabilities. Experimental results show that the transition Péclet number, $Pe_c = R_c/\ell_L$, assumes an almost constant value for the near-equidiffusive acetylene flames with wide ranges in the mixture stoichiometry, oxygen concentration and pressure, where R_c is the flame radius at transition and ℓ_L the laminar flame thickness. However, for the non-equidiffusive hydrogen and propane flames, Pe_c respectively increases and decreases somewhat linearly with the mixture equivalence ratio. Evaluation of Pe_c using previous theory shows complete qualitative agreement and satisfactory quantitative agreement, demonstrating the insensitivity of Pe_c to all system parameters for equidiffusive mixtures, and the dominance of the Markstein number, $Ze(Le-1)$, in destabilization for non-equidiffusive mixtures, where Ze is the Zel'dovich number and Le the Lewis number. The importance of using locally evaluated values of ℓ_L, Ze and Le, extracted from either computationally simulated one-dimensional flame structure with detailed chemistry and transport, or experimentally determined response of stretched flames, in the evaluation of Pe_c is emphasized.

1. Introduction

In the absence of body forces, laminar premixed flames are subjected to two modes of cellular instability; hydrodynamic and diffusional–thermal (Williams 1985; Law 2006). Hydrodynamic instability (Darrieus 1938; Landau 1944) is caused by the density disparity across the flame, represented by, say, the density ratio of the burned to the unburned mixtures, σ, and therefore is present for all flames, while diffusional–thermal instability occurs as a result of the non-equidiffusive properties of the reactive mixture (Sivashinsky 1977, 1983; Clavin 1985), and as such may not be present for flames that are nearly equidiffusive. An appropriate mixture parameter indicating the extent and influence of non-equidiffusion is the global Lewis number, Le, which can be estimated through the ratio of the mixture thermal diffusivity to the mass diffusivity of the limiting reactant relative to the inert which is usually present in abundance, with $Le < 1$, $= 1$ and > 1, respectively, indicating unstable, neutral and stable situations. Furthermore, positive flame curvature, measured in units of the flame thickness, tends to stabilize the hydrodynamic instability, while its influence on the diffusional–thermal instability depends on the nature of the mixture non-equidiffusivity.

The onset of these cellular instabilities is also strongly influenced by the nature and intensity of the global aerodynamic stretch experienced by the flame, with positive stretch tending to be inhibitive (Sivashinsky, Law & Joulin 1982). A prototypical flame configuration that is suitable for a well-controlled study of the governing parameters for the onset of cellularity is the centrally ignited, expanding spherical flame. For this flame configuration it is reasonable to expect, and it has indeed been experimentally observed (Groff 1982; Bradley & Harper 1994; Kwon, Rozenchan & Law 2002; Law, Jomaas & Bechtold 2005), that as the flame expands from the ignition kernel, cellular instability is frequently initially suppressed by the strong curvature-induced stretch associated with the corresponding small flame radii. However, as the flame expands and the stretch intensity lessens, a state is reached at which cell development can no longer be suppressed and consequently cells will appear almost instantaneously over the entire flame surface. This state obviously depends on the combined influences of the hydrodynamic and diffusional–thermal instabilities.

Bechtold & Matalon (1987) and Addabbo, Bechtold & Matalon (2002) successfully analysed the transition to cellularity in expanding spherical flames, and presented an explicit expression for the state of transition as represented by a critical Péclet number, Pe_c, which is the flame radius at transition, R_c, scaled by the laminar flame thickness of the mixture, ℓ_L. Bradley & Harper (1994) subsequently determined the transition state experimentally and found order-of-magnitude agreement with the theoretical predictions. Kwon *et al.* (2002) also performed limited experiments and obtained moderately close agreement with the theory.

The present study was motivated by the recognition that, contrary to the general nature of the theory, an equally comprehensive experimental investigation, together with an appropriate theoretical comparison, had not been conducted. All previous experimental studies have used mixtures that are highly non-equidiffusive, involving fuels species such as hydrogen, propane and iso-octane. The studies on iso-octane by Bradley *et al.* (2000) are particularly noteworthy owing to their quantitative nature, and because the cell development is discussed in detail based on their laser-induced-fluorescence images. However, for all these studies, the flames are non-equidiffusive and are therefore subjected to the combined effects of hydrodynamic and diffusional–thermal instabilities. It thus appears prudent to step back and first identify the transition characteristics of flames subjected only to hydrodynamic instability, using mixtures that are near-equidiffusive. The additional influence of diffusional–thermal instability can then be investigated in a more systematic manner. This constitutes the first objective of the present study, which was accomplished by experimentally determining the critical transition radii for various near-equidiffusive and non-equidiffusive flames, and subsequently examining the response of the corresponding critical Péclet numbers through the use of appropriate laminar flame thicknesses. It will be shown in due course that the present results capture the dominant parametric influences on the transition boundary, in complete agreement with the major features of the theoretical analysis.

Our second objective was to attempt a quantitative comparison between the experimental results and theoretical predictions for the transition boundary. Comparisons of this nature have traditionally been conducted with a fair degree of arbitrariness, especially recognizing the substantial amount of simplification that embodies the theories. However, recent developments have shown that there exists rationalization for such a comparison. Specifically, we first note that many flame phenomena, such as extinction and flame front instability, involve small deviations from the reference adiabatic, planar, steadily propagating premixed flame in the

doubly infinite domain. As a result, the perturbed quantities that describe the relevant flame phenomena are mostly functions of the reference flame, whose properties are conceptually well defined. For example, if the kinetic mechanism and transport properties of a reacting mixture are reasonably well established, then there is confidence in the realism of the computed structure and response of the reference flame. This in turn implies that the perturbed quantities and the associated flame responses can also be predicted with confidence.

An additional consideration is the rational accommodation of certain crucial assumptions in the theory, with a prominent example being the one-step overall reaction characterized by the corresponding overall activation energy. Although it is obvious that such a description cannot be uniformly applied to the diverse thermodynamic states experienced by a flame, such as variations in the system pressure and the mixture equivalence ratio, it is reasonable to expect that it can be locally applied to a single state, provided the global kinetic constants corresponding to the one-step reaction used are also locally defined for that state. The procedure of comparison will be presented.

Finally, it is noted that, from the practical point of view, since spark ignition is central to the operation of many combustion devices, and since the transition to cellularity represents a significantly increased flame propagation rate and consequently bulk heat release rate, the need to understand the roles of the various physico-chemical parameters influencing the transition can hardly be over-emphasized.

In the following we shall first provide a brief overview of the theoretical results, setting the stage for the experimentation and computation. We shall then present the specifics of the experimentation and simulation, as well as the kinetic mechanisms used in the simulation. Thereafter, we present the Péclet number correlation of the experimental results and the comparison with theoretical predictions.

2. Theoretical implications

The linear stability analysis of Bechtold & Matalon (1987), with corrections by Bradley & Harper (1994), and further corrections by Bradley (1999), yields the following expression for the critical Péclet number for transition to cellularity in the presence of both hydrodynamic and diffusional–thermal instabilities,

$$Pe_c = \frac{R_c}{\ell_L} = Pe_1(\sigma) + Ze(Le-1)Pe_2(\sigma), \tag{1}$$

where R_c is the flame radius at transition, $Ze(E_a) = E_a(T_{ad} - T_u)/(R^o T_{ad}^2)$ the Zel'dovich number, E_a the overall activation energy, T_{ad} the adiabatic flame temperature, T_u the free-stream temperature, and R^o the universal gas constant. The first term in (1), Pe_1 (σ), provides the 'base' hydrodynamic boundary between the stretch-affected stable and unstable flame regimes, while the second term describes the additional influence due to diffusional–thermal instability. Thus, Pe_c as a function of equivalence ratio 'pivots' around the 'base' formed for $Le = 1$. It is noted that Pe_c depends only on σ and the wavenumber for pure hydrodynamic instability, manifested for equidiffusive mixtures, and on the additional lumped parameter, $Ma = Ze\,(Le-1)$, for non-equidiffusive mixtures, where Ma is the Markstein number.

A quantitative evaluation of the transition boundary for non-equidiffusive flames would also require a knowledge of several flame parameters in addition to the density ratio σ, namely the adiabatic flame temperature T_{ad}, the laminar flame thickness ℓ_L, the global activation energy E_a, and the global Lewis number Le. Out of these

five parameters, σ and T_{ad} are well-defined quantities for a mixture of given ϕ, T_u and pressure p, and can be readily evaluated. The remaining three parameters are definition dependent, in addition to being dependent on the reference laminar flame and, through it, the state of the mixture. However, they are frequently treated as constants in either theoretical studies or the processing of experimental data. We shall demonstrate shortly that although they are far from being constants, they can nevertheless be evaluated for a given mixture in a rational and consistent manner.

3. Experimental specifications

The experiments were conducted in a dual-chamber apparatus that enables constant-pressure combustion with initial pressures up to 60 atm (Tse, Zhu & Law 2000, 2004). Procedurally, the reactant mixture is prepared in an inner chamber through partial pressures, while the outer chamber is filled with inert gases whose density matches that of the gas in the inner chamber. Two sleeves with holes that are offset relative to one another initially separate the two chambers. Prior to ignition, one sleeve is impulsively slid over the other so that the holes become aligned, allowing the gas in the inner chamber to pass through as the flame propagates. The volume of the outer chamber is 25 times that of the inner chamber, and as a result the pressure rise is less than 3% for the entire chamber. Furthermore, for the small flame radii studied herein, the pressure rise is significantly smaller, resulting in an essentially constant-pressure combustion process. The combustible mixture is spark-ignited at the centre of the inner chamber, with adjustable spark duration between 5 μs and 1 ms. The expanding flame is subsequently quenched as it reaches the separating sleeve, thus preventing the attainment of the large pressure rise usually associated with conventional single-chamber designs. The flame propagation sequence is imaged with schlieren photography and recorded using a high-speed digital motion camera at 8000 f.p.s.

By tracking the thin flame surface before the onset of surface wrinkling, the flame radius can be determined as a function of time, $R(t)$. Since movement of the flame corresponds to that of its downstream boundary, and by allowing for stretch effects that vary with the instantaneous motion of the flame according to the relation (Clavin 1985)

$$s_b = \frac{\mathrm{d}R(t)}{\mathrm{d}t} = s_b^o - L_b\kappa, \tag{2}$$

where s_b^o and L_b are, respectively, the downstream laminar flame speed and the Markstein length, and

$$\kappa(t) = \frac{2}{R(t)}\frac{\mathrm{d}R(t)}{\mathrm{d}t} \tag{3}$$

is the instantaneous strain rate experienced by the flame, the temporal variation of the flame radius is given by (Dowdy *et al.* 1990):

$$R + 2L_b \ln(R) = s_b^o t + \text{constant}. \tag{4}$$

Thus, the instantaneous strain rate $\kappa(t)$ can be readily determined from (3) by using the experimental data on $R(t)$. Furthermore, through regression analysis of $R(t)$ based on (4), the parameters s_b^o and L_b can also be determined. The laminar flame speed based on the upstream condition is then readily given through continuity as $s_u^o = \sigma s_b^o$, which we shall designate as s_L.

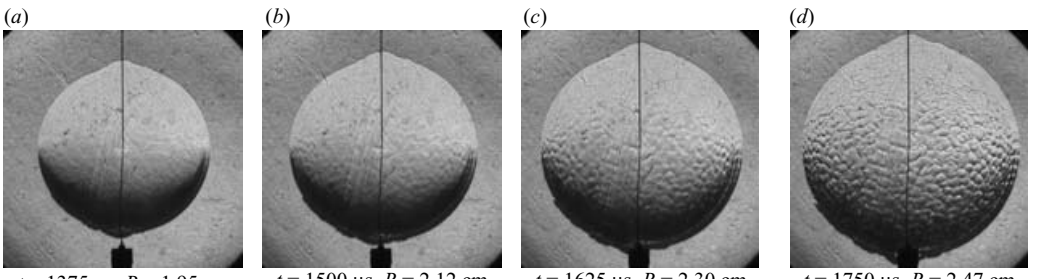

FIGURE 1. Schlieren image sequence of a typical flame propagation showing the transition from a smooth to a cellular flame.

The sequence of flame images was also used to observe the propensity of cell formation and the critical flame radius, R_c, at which cells start to grow. The theoretical framework of Bechtold & Matalon (1987) defines R_c as the radius at which the initial crack occurs on the flame front. Observationally, we have identified this instant as when cells suddenly appear uniformly over the entire flame surface. This instant is rather sharp, and agrees with the general concept of abrupt loss of stability. As an example, figure 1 shows a sequence of images for a typical flame from which figure 1(*b*) would be used to define the critical radius for the onset of instability. Specifically, it is seen that no cells are visible on the flame front in figure 1(*a*), whereas the entire flame is covered with cells in figure 1(*d*). Defining the flame radius in figure 1(*b*) as the critical one yields an uncertainty that is not fully one frame before or after the transition, since figure 1(*a*) has no cells, and figure 1(*c*) clearly shows the presence of cells. The flame propagates with a velocity that corresponds to 0.17 cm per frame, which yields an uncertainty of $\pm 8\%$. We emphasize that this is a very conservative uncertainty estimate, since slower flames cover smaller distances per frame.

It may be noted that large cracks of a permanent structure sometimes appear prior to the uniform onset of cellularity. These large-scale cracks may be attributed to the intrinsic instability, but they are most probably triggered by the ignition event that produces large-amplitude initial disturbances. As such, these structures are the result of a nonlinear hydrodynamic instability and are thus sensitive to the amplitude of the initial disturbance. The subsequent transition of the flame surface to a pebbled surface with cells of more or less comparable size seems to us to be the most appropriate instant to define the onset of instability, at least for the purpose of comparing to the linear theory, which implies that initial disturbances have small (infinitesimal) amplitudes.

We further note that theoretical and numerical analyses have shown that cellular flame fronts can be sensitive to background noises (D'Angelo, Joulin & Boury 2000; Rastigejev & Matalon 2006; Karlin & Sivashinsky 2006). We have endeavoured to eliminate most of the background noise when conducting our experiments. However, noises from the ignition wires and the ignition event could not be eliminated, and could affect the value of the critical radius observed. Although further investigation on the influence of these noises is clearly merited, the regularity and repeatability of our experimental results, and their consistent comparison with the theoretical results obtained without considering these effects, do suggest that their effects could be minimal for the present phenomena.

In the present study, we have used hydrogen and propane as representative non-equidiffusive mixtures with opposite preferential diffusion characteristics. For

near-equidiffusive mixtures, we have used acetylene, which has a molecular weight of 26 and thus is almost diffusively neutral relative to oxygen and nitrogen. Although ethylene has a molecular weight of 28 and hence is slightly more diffusively neutral in air than acetylene, we have used acetylene as our primary fuel because it is more reactive and hence has a smaller flame thickness. Consequently, it has a greater propensity to exhibit hydrodynamic instability. Experiments have nevertheless also been conducted for ethylene, yielding similar results (Jomaas 2005) to those for acetylene.

All experiments were carried out at mixture temperatures of 298 ± 3 K and pressure ranges typically between 4 or 5 and 10 atm. Instabilities were not readily exhibited at lower pressures because of the larger flame thickness, while the upper limit was imposed by safety considerations. Furthermore, only off-stoichiometric mixtures were used at such high pressures. Because of the strong reactivity of the mixtures, especially those of hydrogen and acetylene, these experimental conditions were adequate for inducing the instability phenomena under study.

Estimated experimental uncertainties are $\pm 1\%$ in measuring $R(t)$ and $\pm 8\%$ in determining R_c. The former arises from the pixel resolution of the digital camera, and the latter mainly from the finite framing rate in capturing the instant of transition, especially for small critical radii.

In summary, from the experiments, we can determine for a given mixture its laminar flame speed, s_L, the Markstein length for the burned mixture, L_b, the critical flame radius, R_c, and the associated strain rate at the state of destabilization, κ_c.

4. Computation and kinetic mechanism specifications

As mentioned, properties of the reference laminar flame are required for Péclet number correlations and theoretical comparisons. In addition to experimentation, some of the properties can also be determined from the computed structure and response of these flames. They include the laminar flame speed, s_L, the laminar flame thickness, ℓ_L, and the global activation energy, E_a. Furthermore, the global Lewis number, Le, can be evaluated from the experimental L_b together with E_a and ℓ_L.

The realism of the simulation, however, depends on the accuracy and comprehensiveness of the reaction mechanism used. The present calculations were performed using the PREMIX (Kee *et al.* 1985) one-dimensional flame code, which does not consider instabilities. We perform the calculations with the mechanism of Mueller *et al.* (1999) for hydrogen oxidation and the C_1–C_3 mechanism of Qin *et al.* (2000) for acetylene and propane, hereinafter referred to as the Wang mechanism. The hydrogen mechanism is considered to be adequate for the present study, although the C_1–C_3 mechanism is not uniformly accurate in the prediction of laminar flame speeds, particularly for rich flames (Jomaas *et al.* 2005). Furthermore, this mechanism has not been optimized for $\phi > 1.30$. On the other hand, it is probably the most accurate and comprehensive mechanism available at present, particularly in view of the variety of fuels and the diverse conditions studied herein.

In figures 2 and 3, respectively, we compare the calculated and experimental s_L of acetylene and propane for different ϕ and selected running conditions. The deviations convey a measure of the range of accuracy of the kinetic mechanisms used. Specifically, moderate deviations are observed for acetylene in 15% and 18% O_2 for certain rich equivalence ratios. Similar deviations are observed for propane in air, at pressures of 5 and 10 atm, with the deviation increasing with increasing pressure. The corresponding comparison for hydrogen flames can be found in Tse *et al.* (2000).

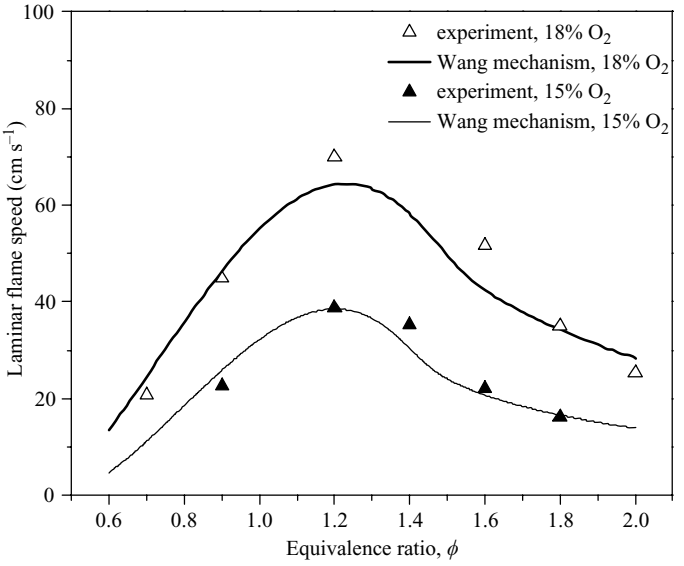

FIGURE 2. Calculated and experimental acetylene (C_2H_2) flame speed in reduced oxygen concentrations at 10 atm; 15% corresponds to $O_2/(O_2+N_2)=0.15$ and 18% corresponds to $O_2/(O_2+N_2)=0.18$.

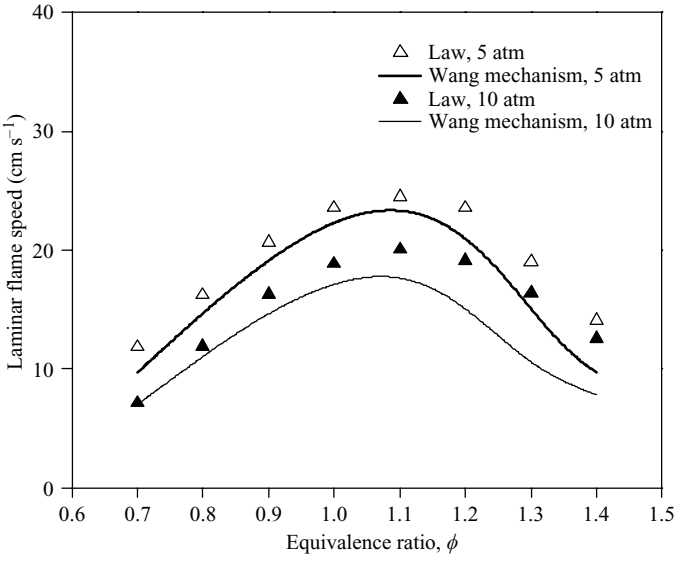

FIGURE 3. Calculated and experimental laminar flame speed for propane (C_3H_8) in air at 5 and 10 atm.

5. Péclet number correlations

5.1. *Evaluation of flame thickness*

The laminar flame thickness is the characteristic length scale that is used to normalize the critical radius in order to obtain Pe_c for the onset of cellular instability. Various definitions have been employed to evaluate ℓ_L, but the present consensus (Poinsot

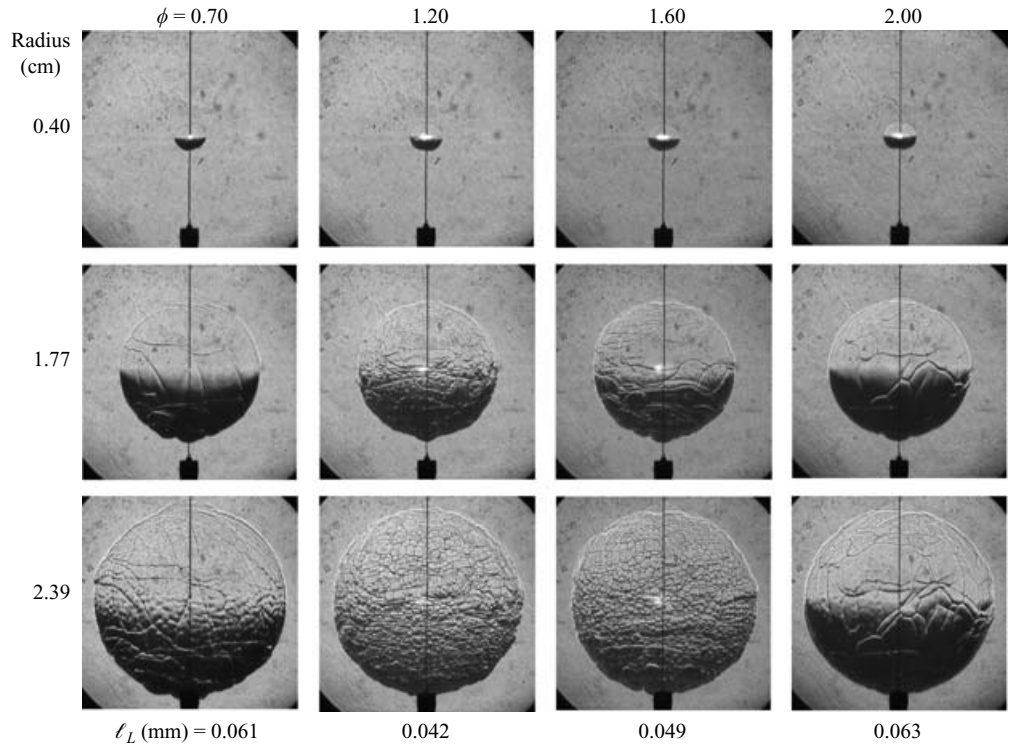

FIGURE 4. Schlieren images of acetylene (C_2H_2) flames in air at 5 atm.

& Veynante 2005) favours the gradient method, defined as

$$\ell_L = \frac{T_{ad} - T_u}{(\mathrm{d}T/\mathrm{d}x)_{max}}, \tag{5}$$

based on the temperature profile of the flame structure. The values so determined have also been found (Sun *et al.* 1999; Law & Sung 2000) to agree closely with those based on the FWHM (full width at half maximum) of the temperature gradient profile, which is another physically reasonable definition. However, we did not find the definition $\ell_L = (\lambda/c_p)/(\rho_u s_L)$ to be useful because of the arbitrariness in the evaluation of the transport parameter λ/c_p. Furthermore, this definition is derived from s_L and as such removes the independent nature of the flame thickness in characterizing the flame behaviour; we shall re-visit this aspect of the flame theory later.

As a final clarification, we want to mention that the expression for flame thickness that appears in the theory is $\lambda/\rho c_p s_L$. However, it is well known that it is difficult to compute reliable values of this expression for real flames because of the ambiguities in determining λ/c_p. Therefore, we have chosen to estimate this quantity using the expression given by (5). This is justified since a straightforward integration of the energy equation across the preheat zone shows that these two expressions are equivalent to first approximation. The quantities appearing in (5) are easily measured and reproducible, and therefore provide a reliable estimate of the flame thickness.

5.2. *Results on near-equidiffusive flames*

We first present results on the near-equidiffusive acetylene flames that are primarily subjected to hydrodynamic instability, with only a minimum dependence on the diffusional–thermal instability. Figure 4 shows the images of expanding flames of

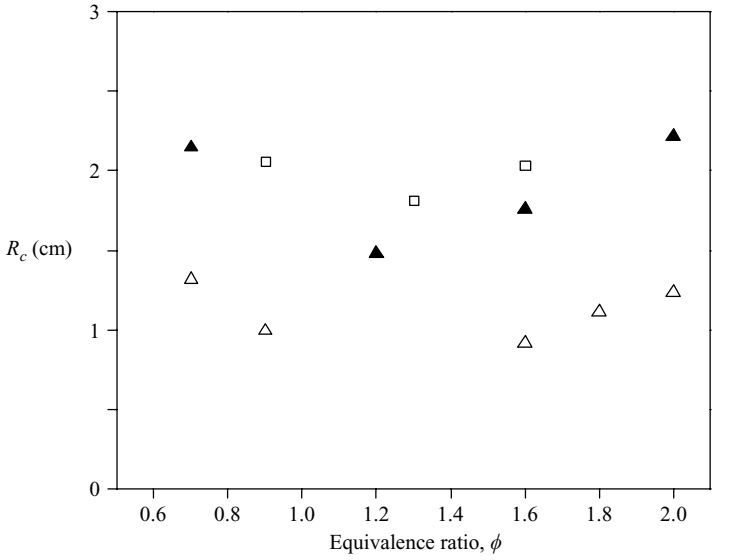

FIGURE 5. Experimental critical radii for onset of instability for acetylene (C_2H_2) in air at □, 4; ▲, 5; △, 10 atm.

acetylene in air at 5 atm, which reveal a non-monotonic trend in the onset of cellularity. That is, destabilization occurs at larger flame sizes for very lean and very rich flames, implying that the flame is more hydrodynamically stable for weaker burning flames, and less stable otherwise. This is physically reasonable as the hydrodynamic instability is expected to be moderated with increasing flame thickness. Since the flame thickness increases as the mixture becomes more off-stoichiometric, on both the lean and rich sides as indicated by the specific values below the images in figure 4, the propensity to destabilize is moderated as well.

To quantify the above observation, figures 5 and 6, respectively, show the experimental R_c and the computed ℓ_L for acetylene flames at 5 atm, and demonstrate the parabolic-like variation for both quantities. From these values, the critical Péclet number, $Pe_c = R_c/\ell_L$, can be evaluated (figure 7). It is seen that, in spite of the significant variations in the propagation velocity and thereby thickness of the flames over the extensive range in ϕ, Pe_c assumes an almost constant value of about 350–375. Referring to (1), this result then suggests that $Pe_1(\sigma)$ is also expected to be a near constant because Pe_c varies primarily with Pe_1 for a near-equidiffusive mixture.

To further explore the near-constant behaviour of Pe_c for near-equidiffusive mixtures, two additional series of experiments were conducted by systematically varying the flame thickness and hence the propensity to destabilize. The second series involves experiments at pressures of 4 and 10 atm, recognizing that the flame thickness is a sensitive function of pressure, whereas Le and σ are not. As such, the flame thickness is the only controlling parameter that changes significantly between different pressures, and this influence should be reflected through the behaviour of the critical radius. Indeed, figures 5 and 6 again exhibit the parabola-like variation of the experimental R_c and calculated ℓ_L at both pressures. When expressed in terms of Pe_c, figure 7 shows that the influence of pressure is scaled out and the data for all pressures at all equivalence ratios again assume a fairly constant value around 350–375.

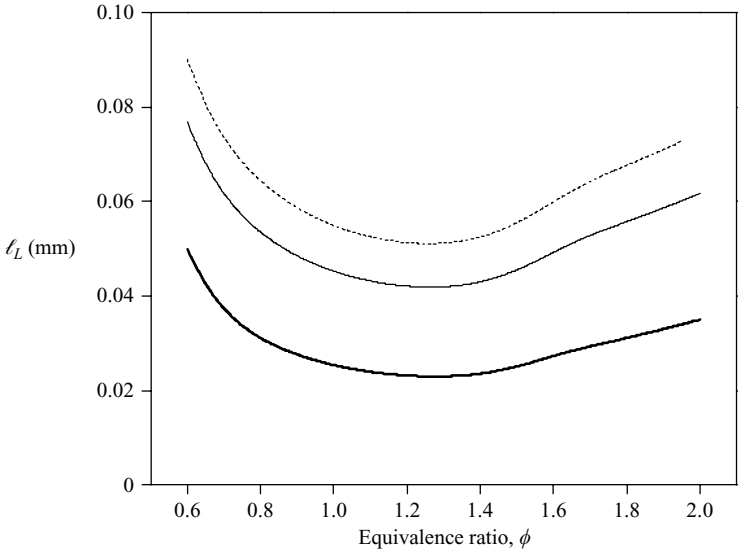

FIGURE 6. Calculated laminar flame thickness for acetylene (C_2H_2) in air at ---, 4; —, 5; ——, 10 atm.

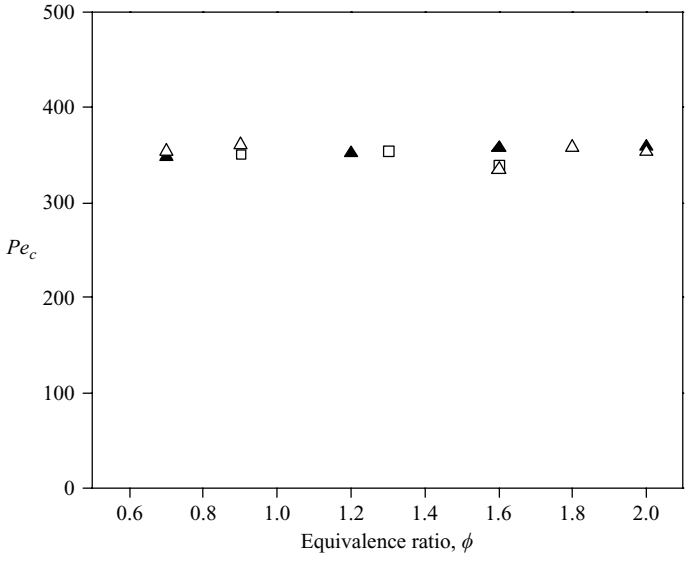

FIGURE 7. Critical Péclet numbers for onset of instability for acetylene (C_2H_2) in air at □, 4; ■, 5; △, 10 atm.

In the third series of experiments, the oxygen concentration in the air was reduced to 18% and 15% by volume, anticipating the sensitive nature with which flame propagation speed and hence the flame thickness depends on the oxidizer concentration. All experiments were conducted at a pressure of 10 atm. Figures 8 and 9 then show the experimental R_c and the calculated ℓ_L for all the oxidizer concentrations including that of air, while figure 10 shows the corresponding Pe_c. It can be seen that Pe_c again assumes the fairly constant value of 350–375, up to $\phi \approx 1.3$. For higher ϕ the spread is larger, but Pe_c is nevertheless still bounded within

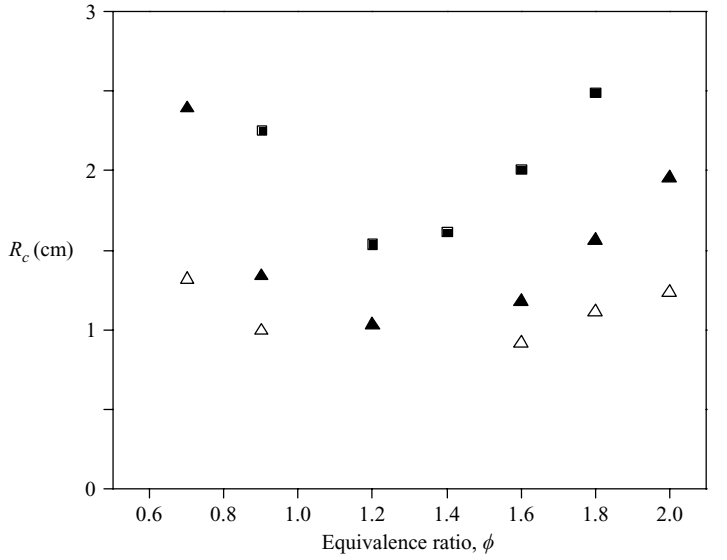

FIGURE 8. Experimental critical radii for onset of instability for acetylene (C_2H_2) with different oxygen/nitrogen concentrations at 10 atm. ■, 15% O_2 in air; ▲, 18% O_2 in air; △, 21% O_2 in air.

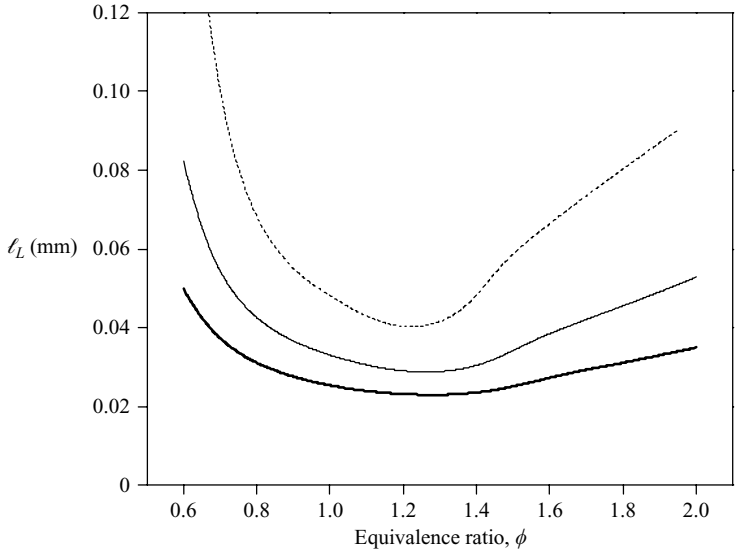

FIGURE 9. Calculated laminar flame thickness for acetylene (C_2H_2) with different oxygen/nitrogen concentrations at 10 atm. - - -, 15% O_2 in air; —, 18% O_2 in air; —, 21% O_2 in air.

a narrow range of 300–375. As cautioned earlier, there is a greater uncertainty in the kinetic mechanism for such high-ϕ mixtures, and this could be reflected in the larger scatter in Pe_c through ℓ_L for mixtures with lower oxygen concentrations. In particular, figure 2 shows an underestimate of the calculated laminar flame speed in 18% oxygen in the approximate range of $\phi = 1.2-1.8$. As a result, the flame thickness is overestimated which in turn causes the small dip in Pe_c for this range of ϕ as compared to other results.

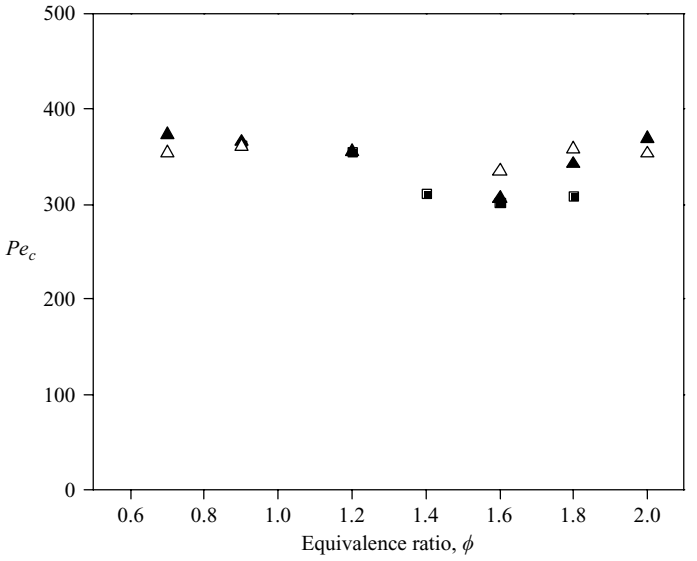

FIGURE 10. Critical Péclet number for onset of instability for acetylene (C_2H_2) with different oxygen/nitrogen concentrations at 10 atm. ■, 15% O_2 in air; ▲, 18% O_2 in air; △, 21% O_2 in air.

5.3. *Results on non-equidiffusive flames*

Now we present results on non-equidiffusive flames that are subjected to both hydrodynamic and diffusional–thermal instabilities, recognizing that, for the fuels used, $Le > 1$ for lean propane and rich hydrogen flames, whereas $Le < 1$ for rich propane and lean hydrogen flames. Figure 11 shows the images of the lean and rich flames of hydrogen and propane in air at 5 atm. As expected, and also in agreement with previous observations (Bradley & Harper 1994; Law *et al.* 2005), the development of diffusional–thermal cells is promoted for flames in which the deficient reactant is also the more diffusive one such that $Le < 1$. Groff (1982) attributed the cellular pattern in rich propane flames at the same pressure to hydrodynamic effects, although it is obvious that diffusional–thermal effects impose an additional destabilizing effect. This possibility is substantiated by comparing the lean and rich propane flames in figure 11, which shows that while both flames have about the same σ, the rich flame is thicker and hence is less susceptible to hydrodynamic instability. Thus the presence of wrinkles over rich flames must be the consequence of the destabilizing, $Le < 1$, non-equidiffusion effect, while the absence of wrinkles over lean flames is the consequence of the stabilizing, $Le > 1$, non-equidiffusion effect. The same observation can be made for hydrogen flames, except the responses of lean and rich flames are reversed.

We next present results on the Pe_c determined for these non-equidiffusion flames. The trends for these non-equidiffusive flames are similar to those observed for Pe_c by Gu *et al.* (2000).

Propane flames

The critical radius for the onset of instability and the calculated flame thickness for propane flames at 5 and 10 atm are shown in figure 12. We can see that ℓ_L decreases with pressure, and has a minimum in terms of ϕ for slightly rich mixtures, corresponding to where the laminar flame speed is the largest. These thicknesses

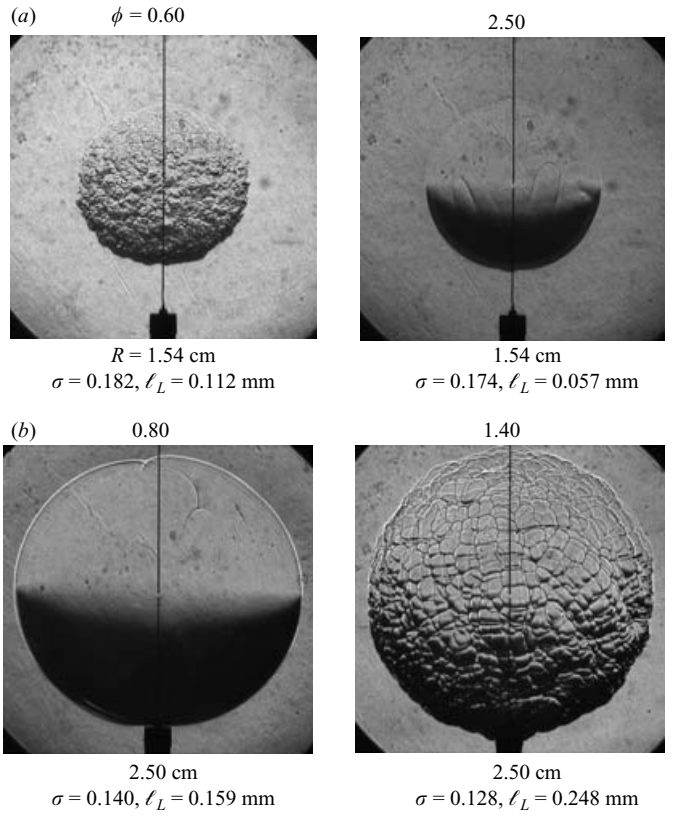

FIGURE 11. Schlieren images of (*a*) lean and rich hydrogen (H_2) and (*b*) propane (C_3H_8) flames at 5 atm.

are similar to those of the near-equidiffusion flames, and control the onset of hydrodynamic instability. However, contrary to the 'parabolic' result for the near-equidiffusion acetylene flames, the experimental R_c for propane flames monotonically decreases with increasing ϕ, from $\phi = 1.0$ to 1.4. This is clearly a manifestation of the destabilizing non-equidiffusion influence for these primarily $Le < 1$ mixtures, causing the flame to become unstable at smaller radius and hence stronger stretch, and with its influence increasing as the flame becomes weaker.

There are no data for lean flames because for such flames both the flame thickness and the stable ($Le > 1$) diffusional–thermal properties contribute to flame stability. Consequently, the critical radii are larger than the largest observable radius (3 cm) in the experiment, being limited by the schlieren set-up.

Figure 13 then shows the variation of Pe_c with ϕ for the propane flames. In contrast to the near-equidiffusive flames, Pe_c now shows a moderately linear decreasing trend with increasing equivalence ratio. From the results on near-equidiffusive flames, we expect Pe_c to be approximately 350 for the equivalence ratio at which Le for propane is close to unity. Using this value, figure 13 shows that the flame behaviour approaches that of unity Le for equivalence ratios slightly on the lean side, which agrees well with results from previous studies of stretched propane Bunsen flames (Law *et al.* 1988). Figure 13 also shows that Pe_c varies only weakly with pressure. Since the flame thickness does vary substantially with pressure, this insensitivity not only demonstrates

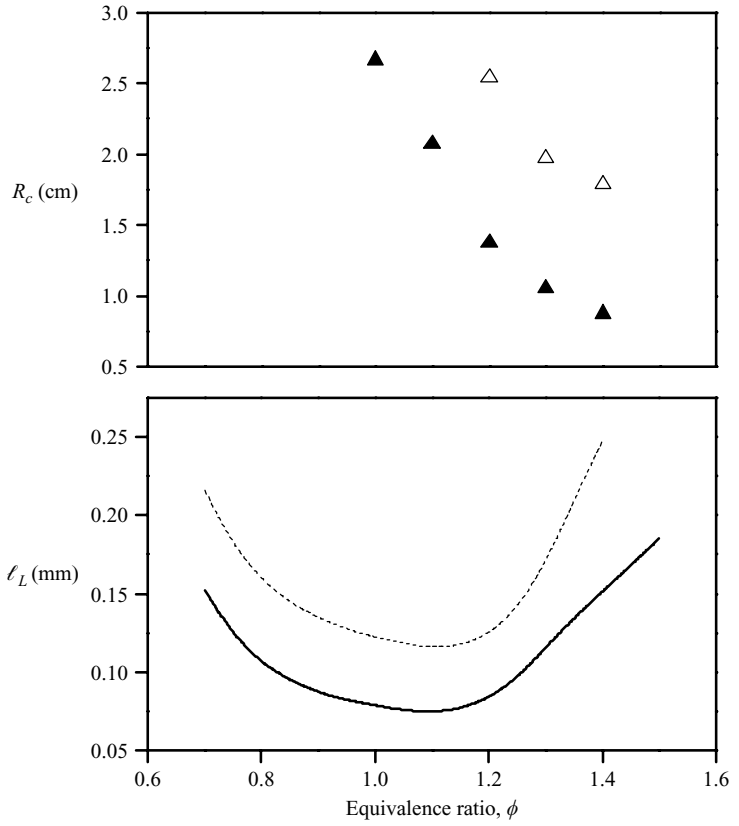

FIGURE 12. Critical radii for onset of instability and computed flame thickness for propane (C_3H_8) in air at △, - - -, 5 atm; ▲, —, 10 atm.

the correctness in the scaling for the transition radius, but also emphasizes again the need to use local values such as the flame thickness in evaluating Pe_c.

Hydrogen flames

Figure 14 shows R_c and ℓ_L for hydrogen flames at 5 atm. Since the Le of hydrogen flames increases as ϕ increases – a trend that is opposite to that for propane flames – the critical radius is smallest for very lean flames.

The opposite diffusional–thermal properties for the hydrogen and propane flames are clear when the Pe_c of hydrogen are compared to those for propane (figure 13). It is seen that the Pe_c is approximately 350 at $\phi \sim 1.50$, indicating that equidiffusion is attained near this ϕ. Noting that the maximum flame speed of hydrogen–air mixtures occurs around $\phi \sim 1.8$, where the hydrodynamic instability is expected to be the strongest, the shifting to a lower ϕ indicates the exertion of the stabilizing diffusional–thermal effect on cell development.

6. Theoretical evaluation and comparison of Pe_c

The above results on the Pe_c correlation show that while Pe_c varies minimally with ϕ for the near-equidiffusive flames of acetylene, it increases and decreases with ϕ fairly substantially for the non-equidiffusive flames of hydrogen and propane, respectively.

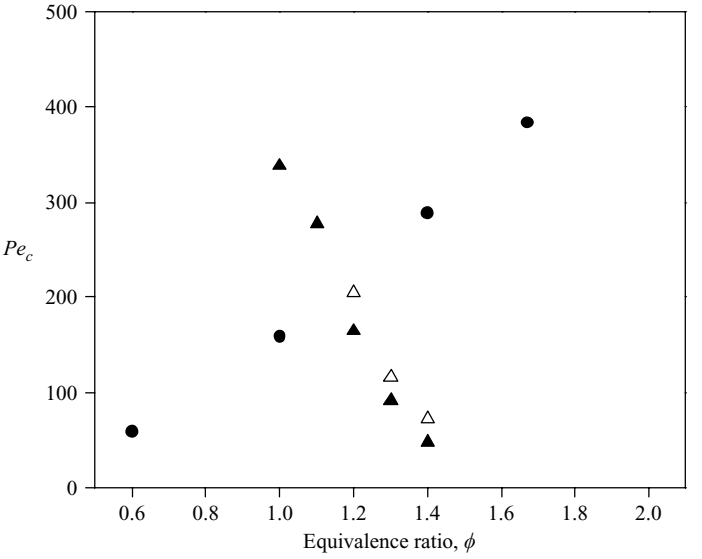

FIGURE 13. Critical Péclet number for onset of instability for propane (C_3H_8) in air at △, 5 and ▲, 10 atm and ●, for hydrogen (H_2) in air at 5 atm.

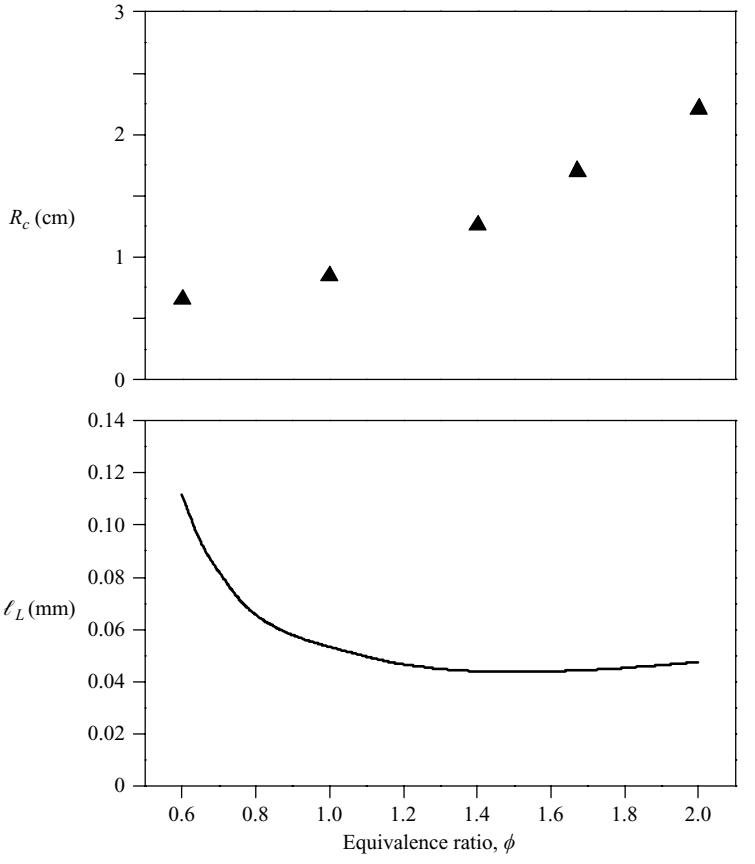

FIGURE 14. Critical radii for onset of instability and computed flame thickness for hydrogen (H_2) in air at 5 atm.

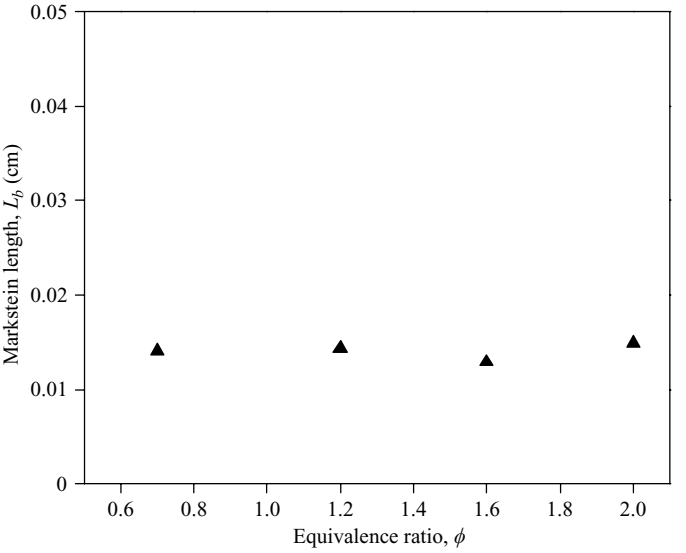

FIGURE 15. Markstein lengths for acetylene (C_2H_2) in air at 5 atm.

We shall now study this in the light of the theoretical predictions of Bechtold & Matalon (1987).

6.1. *Extraction of activation energy and Lewis number*

As mentioned earlier, an independent evaluation of the theoretical predictions for Pe_c requires knowledge of the global Lewis number, Le, and the Zel'dovich number, Ze, which in turn depends on the global activation energy, E_a. Following Egolfopoulos & Law (1990), E_a can be readily determined from

$$\frac{E_a}{R_0} = -2\left[\frac{\partial \ln(\rho_u s_L)}{\partial(1/T_{ad})}\right]_{p,\phi}. \tag{6}$$

The differential can be evaluated by calculating $\rho_u s_L$ for the given p and ϕ, and by slightly varying its value through, say, the substitution of a small quantity of the nitrogen by inert argon.

To evaluate Le, we note that it is related to Ze, σ, ℓ_L and L_b through (Bechtold & Matalon 2001)

$$\frac{L_b}{\ell_L} = \sigma\gamma_1 + \tfrac{1}{2}(Le-1)Ze\gamma_2, \tag{7}$$

where γ_1 and γ_2 are functions of σ, and L_b can be determined experimentally, as shown in figure 15 for acetylene flames. Note that σ is smaller than unity in our definition, whereas Bechtold & Matalon (2001) uses the reciprocal of the σ used herein.

Figure 16 then shows the extracted Le for acetylene flames at representative conditions. Since the extraction is based on the effect of stretch on the flame speed, which is a higher-order quantity as compared to, say, the flame speed and thickness, the extracted values of Le have larger scatters. These data, however, do show that the Le for acetylene is close to unity and is almost insensitive to ϕ.

The Lewis numbers for hydrogen and propane flames have been previously determined (Sun *et al.* 1999; Law & Sung 2000), and, respectively, show monotonically

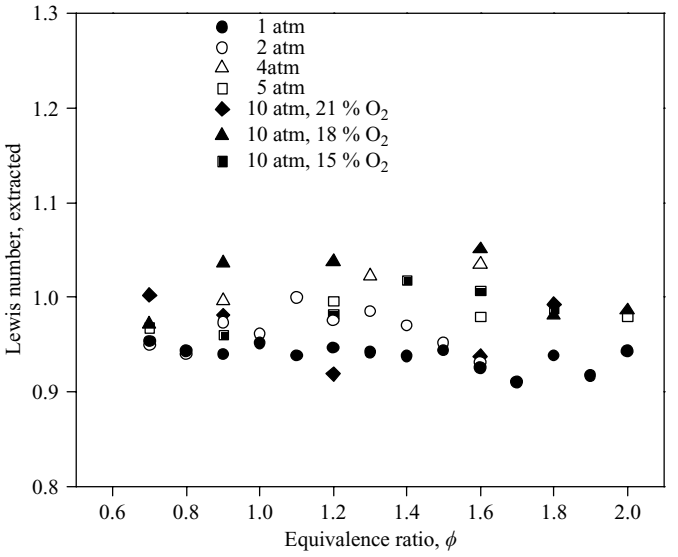

FIGURE 16. Extracted Lewis number for acetylene (C_2H_2) in air at various running conditions.

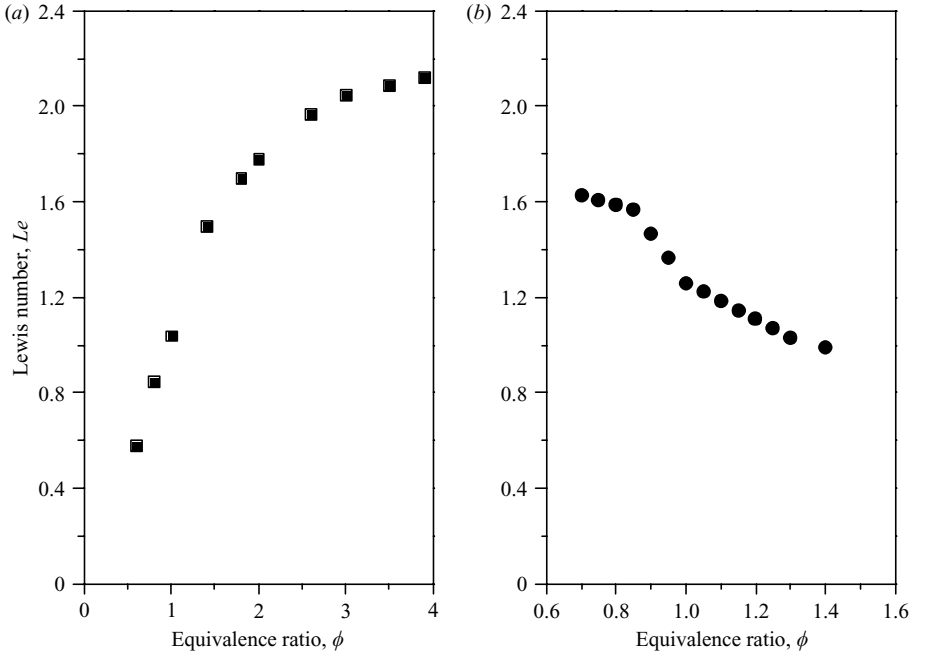

FIGURE 17. Lewis number as a function of equivalence ratio for (*a*) hydrogen (H_2) and (*b*) propane (C_3H_8) in air.

increasing and decreasing values as ϕ increases from lean to rich (figure 17), as expected. These values will be used as reported.

Figure 18 shows the extracted global activation energy, E_a, for the acetylene, hydrogen and propane flames, at 5 atm. It can be seen that the E_a for propane decreases and then increases with ϕ, with the trend reversing around, but slightly

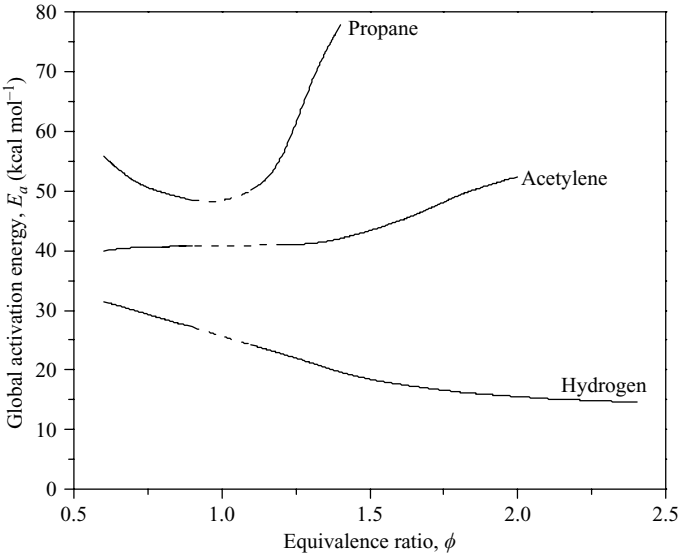

FIGURE 18. Global activation energy for acetylene (C_2H_2), hydrogen (H_2), and propane (C_3H_8) in air at 5 atm.

leaner than, the stoichiometric concentration. This behaviour reflects the controlling influence of the flame temperature, which peaks around stoichiometric and facilitates the temperature-sensitive two-body branching reactions relative to the temperature-insensitive three-body termination reactions, leading to overall faster reactions around stoichiometric and thereby reduced global activation energies there.

For hydrogen flames, the same 'parabolic' behaviour is observed, with the increasing trend exhibited for values of ϕ larger than those shown in the figure. The range of the minimum values of E_a, however, is around $\phi = 1.7$ to 2.1 instead of stoichiometric where the flame temperature peaks. Recognizing that the flame speed also peaks around this range as a result of the large value of the *Le* for rich mixtures, and since the global activation energy was extracted from the response of the flame speed, this rich shifting of the minimum E_a is therefore a consequence of non-equidiffusion. Note that this result demonstrates the intrusion of transport on a supposedly chemical property when the system is affected by transport.

We also note that the values of E_a around stoichiometry are interpolated for all curves. This is because its extraction based on (6) holds only for sufficiently off-stoichiometric mixtures for which the reaction rate is controlled by the deficient reactant. A brute-force, and incorrect, extraction using (6) will yield an increasing trend towards stoichiometry, indicating effects due to the progressively reduced concentration of the limiting reactant.

6.2. *Comparison*

We first consider the near-equidiffusive flames of acetylene. Figure 19 plots the theoretical and experimental Pe_c for acetylene in air at 5 atm, showing good qualitative agreement and satisfactory quantitative agreement. In particular, we note the fairly insensitive nature of Pe_c with variations in ϕ. Similar behaviour was also observed for burning at other pressures and oxygen concentrations.

To understand the cause for the near-constant value of Pe_c, we analyse the hydrodynamic component $Pe_1(\sigma)$. We first note that for practical combustion systems,

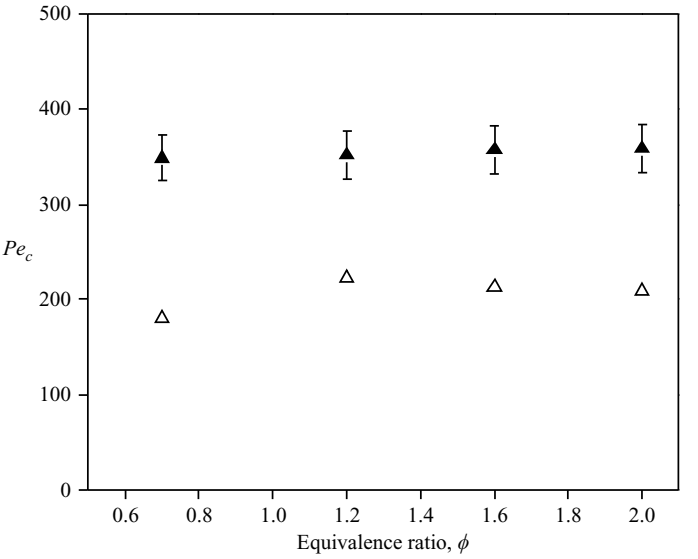

FIGURE 19. Experimental (▲) and theoretical (△) critical Péclet numbers for acetylene (C_2H_2) in air at 5 atm.

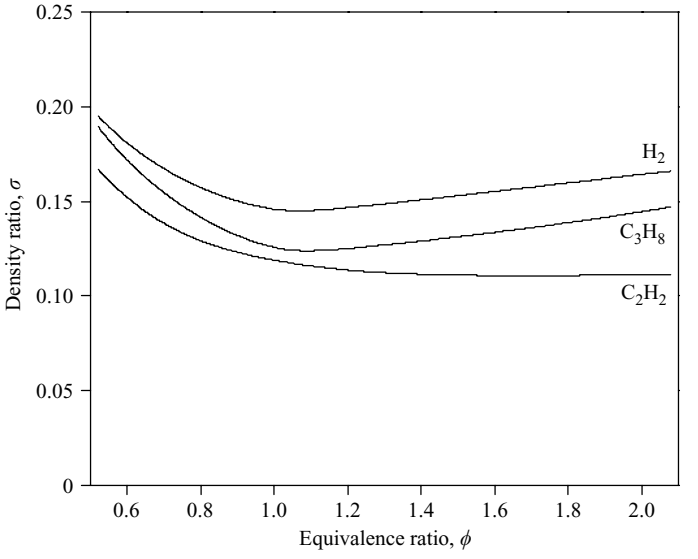

FIGURE 20. Density ratio for acetylene (C_2H_2), propane (C_3H_8), and hydrogen (H_2) in air.

σ is typically a small number, indicating the associated strong exothermicity. Figure 20 shows their values for the three fuel systems to be studied, namely acetylene, hydrogen and propane in atmospheric air. It is seen that within the extensive range of the equivalence ratio $0.5 < \phi < 2.0$, σ varies between 0.1 and 0.2. Figure 21 then plots the function $Pe_1(\sigma)$ for $0.1 < \sigma < 0.2$, evaluated at the critical value of the wavenumber, n_c, which is a function of σ. The variation of $Pe_1(\sigma)$ over this range is rather moderate. Furthermore, since the variation of σ over the flammable range is quite restricted for a given hydrocarbon fuel, varying for example between 0.11 and 0.17 for acetylene, the extent of variation of $Pe_1(\sigma)$ over the flammable range is further restricted. We thus

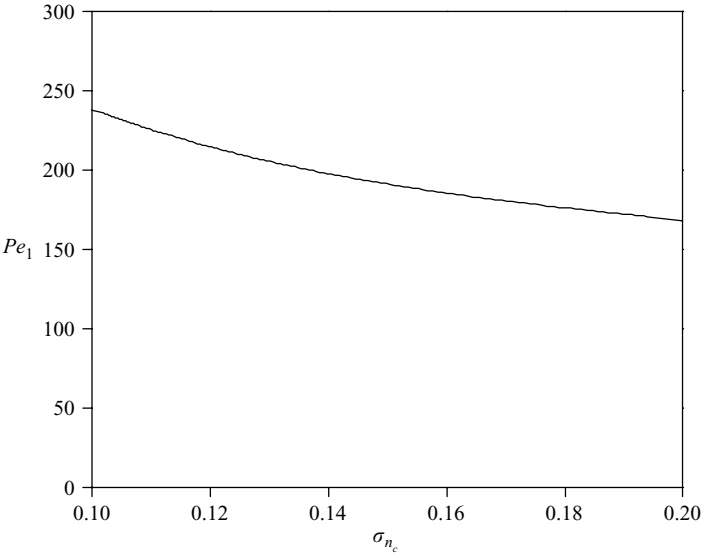

FIGURE 21. Pe_1 as a function of the density ratio, σ, evaluated at the critical wavenumber, n_c.

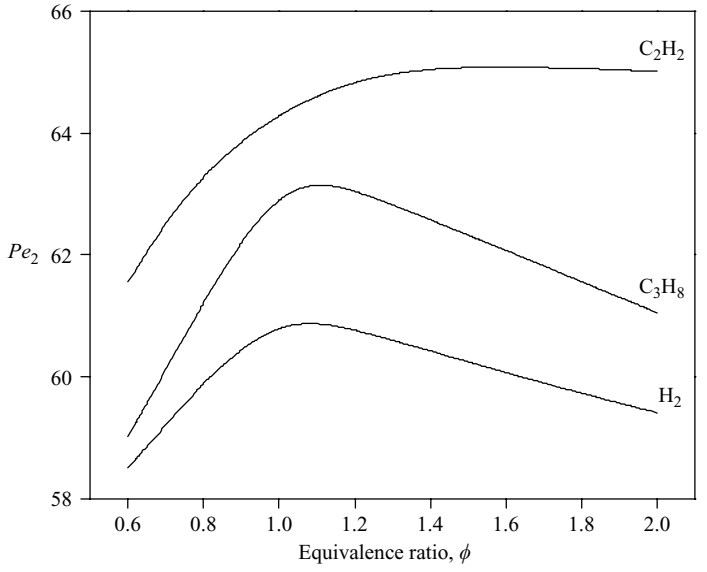

FIGURE 22. Pe_2 as a function of equivalence ratio for acetylene (C_2H_2), hydrogen (H_2), and propane (C_3H_8) at 5 atm.

arrive at the important observation that the transition boundary for hydrodynamic instability, for equidiffusive flames, in terms of the critical Péclet number, Pe_c, varies over a very narrow numerical range, being insensitive to the specific as well as all system parameters. Our results show that this value is around 200.

We next inspect the behaviour of the non-equidiffusive term, $Ze\,(Le-1)\,Pe_2(\sigma)$, in (1) because it also contributes to the overall stability. To identify the role of the individual factors constituting this term, we have plotted in figures 22, 23 and 24 the variations of $Pe_2(\sigma)$, Ze and $Ze(Le-1)$, respectively. It is seen that, similar to $Pe_1(\sigma)$,

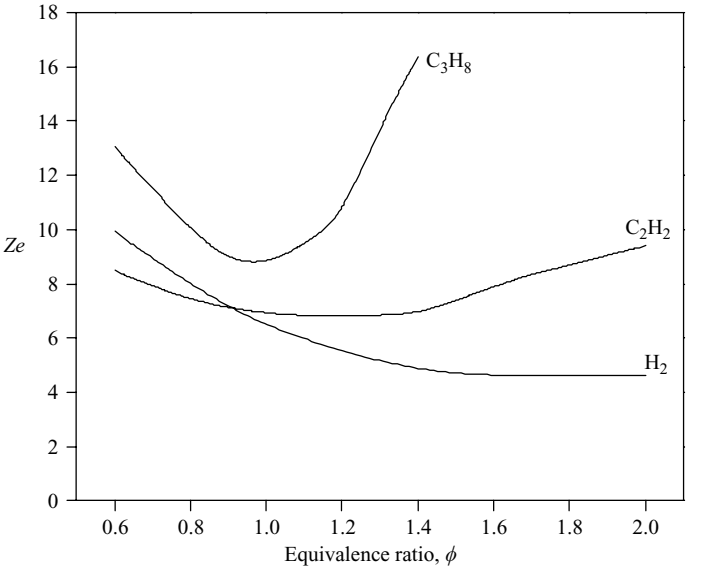

FIGURE 23. Zeldovich number, Ze, as a function of equivalence ratio for acetylene (C_2H_2), hydrogen (H_2), and propane (C_3H_8) in air at 5 atm.

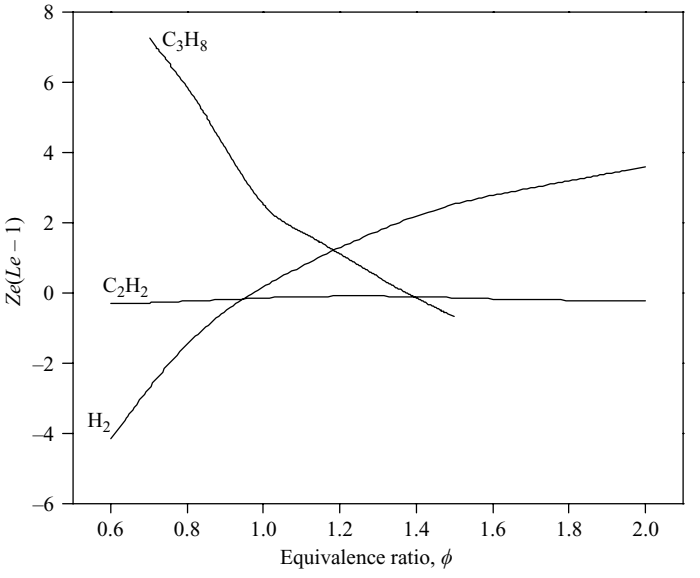

FIGURE 24. $Ze(Le-1)$ as a function of equivalence ratio for acetylene (C_2H_2), hydrogen (H_2), and propane (C_3H_8) in air at 5 atm.

$Pe_2(\sigma)$ also varies minimally with ϕ. For the near-equidiffusive acetylene flame, the variation of Ze is also not large. Thus, when Ze is combined with $(Le-1)$ for the acetylene flames, with Le itself being close to unity and insensitive to ϕ, the factor $Ze(Le-1)$ varies minimally. These results explain the near constant value of the non-equidiffusive term for acetylene flames, and consequently the correspondingly near constant value of its transition Péclet number.

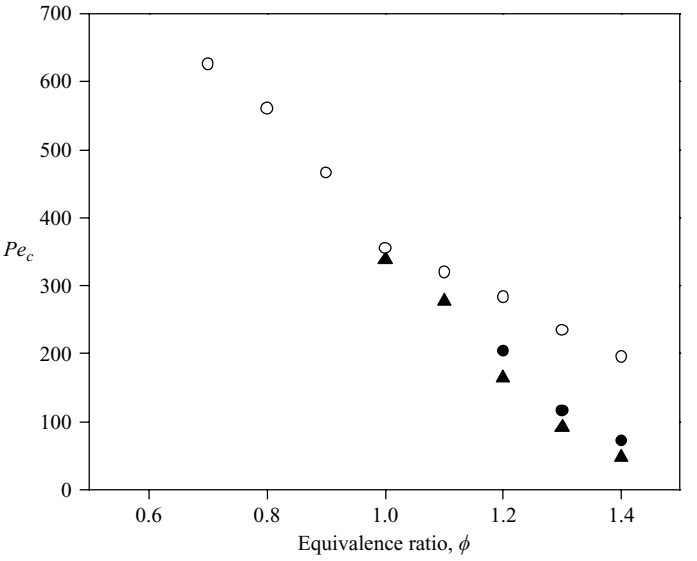

FIGURE 25. Experimental and theoretical critical Péclet numbers for propane (C_3H_8) in air. ○, 5 atm, theory; ●, 5 atm; ▲, 10 atm.

To conduct a comparison for the non-equidiffusion mixtures, we first note that since both $Pe_1(\sigma)$ and $Pe_2(\sigma)$ are insensitive to σ, the dependence of Pe_c on the state of the mixture must mostly come from the term representing $Ze(Le-1)$, as shown in figure 24.

Figure 25 then shows the comparison for propane in air at 5 and 10 atm. To avoid clutter, the theoretical values at 10 atm, which are almost identical to those at 5 atm, are not included in the plot. It is first seen that the decreasing trend of Pe_c with ϕ is captured. Furthermore, since Ze varies non-monotonically with ϕ (figure 23), while $Ze(Le-1)$ decreases with ϕ (figure 24), it is the decreasing trend of Le with ϕ (figure 17) that effects the decreasing trend of Pe_c, which is reasonable. The calculated result of the moderate insensitivity of Pe_c with pressure also substantiates the experimental observation. This is again reasonable because Le and σ are both insensitive to pressure, while the influence of Ze is also not large.

Figure 26 compares the theoretical and experimental Pe_c for hydrogen at 5 atm, and shows that not only is the increasing trend of Pe_c with ϕ captured, the values are also numerically close. As seen from figures 17, 23 and 24, this increasing trend is again due to the corresponding increase of Le.

While the comparison between the experimental and theoretical Pe_c can be considered to be satisfactory for the non-equidiffusive flames, there do exist some discernible second-order differences. In particular, for propane flames, the theoretical values are not only higher, but also exhibit a slower variation with ϕ such that the deviation becomes large at larger ϕ. For hydrogen flames, the theoretical values show a fairly discernible nonlinearity, causing a slight bending down of the Pe_c with increasing ϕ, indicating a weaker influence as the mixture becomes progressively more diffusional–thermally stable. These results then indicate that the further away from the diffusively neutral situation, the stronger is the influence of diffusional–thermal instability than described by the theory. As a result, the theory slightly overpredicts the stability of $Le < 1$ flames and underpredicts the stability of $Le > 1$ flames.

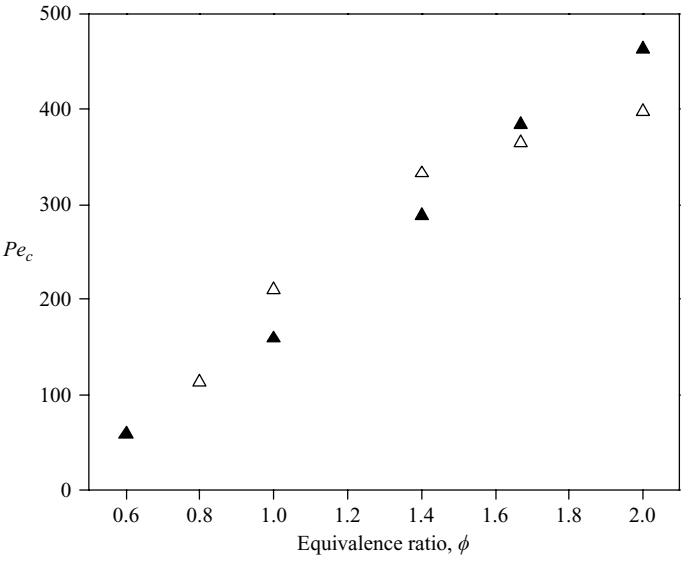

FIGURE 26. Experimental (▲) and theoretical (△) critical Péclet numbers for hydrogen (H_2) in air at 5 atm.

We close this discussion on the comparison between theory and experiment by cautioning that very close quantitative agreement in comparison is not to be expected, for several reasons. First, the theory itself is asymptotic, based on the largeness of Ze. Hence, neglect of higher-order terms would contribute to an inherent inaccuracy. Since Ze is typically around 10 but can be as small as 5, (figure 23), inaccuracy of the order of 10–20% is to be expected. Secondly, and perhaps most important, is the definition of the flame thickness. Clearly, 'fine tuning' of the definition can lead to closer agreement, but we believe the gradient definition has so far shown its appropriateness for a variety of flame phenomena and should be used consistently. The third factor is the accuracy in the extraction of the global Le. As mentioned earlier, since its extraction from experimental data on the flame radius history involves its derivative, the accuracy is reduced. The final factor is the inaccuracy of the kinetic mechanisms used in the flame calculations. This will improve as better mechanisms are developed over time.

In spite of the above reservations, it is nevertheless important to emphasize that, considering the complexity of the phenomena and the extensive nature of the present investigation in terms of parametric variations, the degree of agreement is internally consistent and indeed is rather satisfactory.

7. Concluding remarks

In the present study we have conducted a fairly comprehensive investigation on the onset of cellularity of the positively stretched, outwardly propagating spherical flame owing to hydrodynamic and diffusional-thermal instabilities. The separate and combined influences of these instabilities were systematically identified by using acetylene as a near-equidiffusive fuel, and hydrogen and propane as representative non-equidiffusive fuels that respectively become less and more stable with increasing fuel concentration. The influence of hydrodynamic instability was further manipulated

by varying the mixture pressure and oxygen concentration, which affect the flame thickness and hence the curvature-induced stabilization tendency.

Perhaps the most important understanding gained from the present study is the need to use proper system parameters in the interpretation of the experimental data and their subsequent comparison with the theoretical predictions. Such recognition occurred at two levels of data reduction. The first is the use of the appropriate flame thickness, ℓ_L, determined from the real flame structure, in evaluating the critical Péclet number. It is obvious that had a constant ℓ_L been used, as is frequently done, a non-monotonic parabolic response instead of a near-constant response would have been observed for the near-equidiffusive acetylene flames, leading to considerable confusion in an attempt to reconcile with the theoretical prediction. The second level of recognition is the use of extracted values for the global activation energy and Lewis number in the data reduction for the non-equidiffusive hydrogen and propane flames.

The above recognitions further substantiate the two corollary understandings of the proper interpretation of the laminar flame properties (Law & Sung 2000). First, the parameter ℓ_L is as important as the laminar flame speed, s_L, in characterizing the reference one-dimensional planar premixed flame. Indeed, since laminar flame propagation is controlled by the two processes of diffusion and reaction, its global response should also be characterized by two parameters, whether they are the diffusivity and reactivity of the flame, or s_L and ℓ_L. As such, ℓ_L should be determined independent of s_L. The conventional specification of ℓ_L through the relation $(\lambda/c_p)/s_L$ has implicitly used λ/c_p and s_L as the two flame parameters, leading ℓ_L to be a derived quantity.

The second understanding is that the system Lewis number is a global parameter of the flame, not of the free-stream mixture. As such, it must be extracted from properties pertaining to the flame, just as the activation energy is a global parameter of the flame that must be properly extracted.

Finally, it is hoped that the present study provides a rational framework for the quantitative description of the dynamics of laminar flames, based on flame theories using global large activation reactions and Lewis numbers.

The work at Princeton University was supported by the NASA microgravity combustion program and a block grant from BP and Ford on carbon mitigation and hydrogen economy. We thank Dr Jiao Yuan and Mr Delin Zhu for their assistance. Discussions with Professor Stephen Tse of Rutgers University about the experimental set-up were helpful, and very much appreciated.

REFERENCES

Addabbo, R., Bechtold, J. K. & Matalon, M. 2002 Wrinkling of spherically expanding flames. *Proc. Combust. Inst.* **29**, 1527–1535.

Bechtold, J. K. & Matalon, M. 1987 Hydrodynamic and diffusion effects on the stability of spherically expanding flames. *Combust. Flame* **67**, 77–90.

Bechtold, J. K. & Matalon, M. 2001 The dependence of the Markstein length on stoichiometry. *Combust. Flame* **127**, 1906–1913.

Bradley, D. 1999 Instabilities and flame speeds in large-scale premixed gaseous explosions. *Phil. Trans. R. Soc. Lond.* A **357**, 3567–3581.

Bradley, D. & Harper, C. M. 1994 The development of instabilities in laminar explosion flames. *Combust. Flame* **99**, 562–572.

Bradley, D., Sheppard, C. G. W., Woolley, R., Greenhalgh, D. A. & Lockett, R. D. 2000 The development and structure of flame instabilities and cellularity at low Markstein numbers in explosions. *Combust. Flame* **122**, 195–209.

Clavin, P. 1985 Dynamic behavior of premixed flame fronts in laminar and turbulent flows. *Prog. Energy Combust. Sci.* **11**, 1–59.

D'Angelo, G., Joulin, G. & Boury, G. 2000 On model evolution equations for the whole surface of three-dimensional expanding wrinkled premixed flames. *Combust. Theory Modelling* **4**, 317–338.

Darrieus, G. 1938 Propagation d'un front de flamme. *La Technique Moderne* **30**, no. 18.

Dowdy, D. R., Smith, D. B., Taylor, S. C. & Williams, A. 1990 The use of expanding spherical flames to determine burning velocities and stretch effects in hydrogen/air mixtures. *Proc. Combust. Instit.* **23**, 325–333.

Egolfopoulos, F. N. & Law, C. K. 1990 Chain mechanisms in the overall reaction orders in laminar flame propagation. *Combust. Flame* **80,** 7–16.

Groff, E. G. 1982 The cellular nature of confined spherical propane-air flames. *Combust. Flame* **48**, 51–62.

Gu, X. J., Haq, M. Z., Lawes, M. & Woolley, R. 2000 Laminar burning velocity and Markstein lengths of methane-air mixtures. *Combust. Flame* **121**, 41–58.

Jomaas, G. 2005 An experimental study on the laminar burning velocities and stability boundaries of outwardly propagating spherical flames. MSE thesis, Princeton University.

Jomaas, G., Zheng, X., Zhu, D. L., & Law, C. K. 2005 Experimental determination of counterflow ignition temperatures and laminar flame speeds of C_2–C_3 hydrocarbons at atmospheric and elevated pressures. *Proc. Combust. Inst.* **30**, 193–200.

Karlin, V. & Sivashinsky, G. 2006 The rate of expansion of spherical flames. *Combust. Theory Modelling* **10**, 625–637.

Kee, R. J., Grcar, J. F., Smooke, M. D. & Miller, J. A. 1985 A Fortran program for modeling steady laminar one-dimensional premixed flames. *Sandia. Rep.* SAND85-8240.

Kwon, O. C. & Faeth, G. M. 2001 Flame/stretch interactions of premixed hydrogen-fueled flames: measurements and predictions. *Combust. Flame* **124**, 590–610.

Kwon, O. C., Rozenchan, G. & Law, C. K. 2002 Cellular instabilities and self-acceleration of outwardly propagating spherical flames. *Proc. Combust. Instit.* **29**, 1775–1784.

Landau, L. D. 1944 On the theory of slow combustion. *Acta Physicochim. URSS* **19**, 77–85.

Law, C. K. 2006 *Combustion Physics.* Cambridge University Press.

Law, C. K. & Sung, C. J. 2000 Structure, aerodynamics, and geometry of premixed flamelets. *Prog. Energy Combust. Sci.* **26**, 459–505.

Law, C. K., Cho, P., Mizomoto, M. & Yoshida, H. 1988 Flame curvature and preferential diffusion in the burning intensity of Bunsen flames. *Proc. Combust. Instit.* **21**, 1803–1809.

Law, C. K., Jomaas, G. & Bechtold, J. K. 2005 Cellular instabilities of expanding hydrogen/propane spherical flames at elevated pressure: theory and experiment. *Proc. Combust. Instit.* **30**, 159–167.

Markstein, G. H. (ed.) 1964 *Non-steady Flame Propagation.* Pergamon.

Mueller, M. A., Kim, T. J., Yetter, R. A. & Dryer, F. L. 1999 Flow reactor studies and kinetic modeling of the H_2/O_2 reaction. *Intl J. Chem. Kinet.* **31**, 113–125.

Poinsot, T. & Veynante, D. 2005 *Theoretical and Numerical Combustion.* R. T. Edwards, Flourtown.

Qin, Z., Lissianski, V., Yang, H., Gardiner, W. C., Davis, S. G. & Wang, H. 2000 Combustion chemistry of propane: a case study of detailed reaction mechanism optimization. *Proc. Combust. Inst.* **28**, 1663–1669.

Rastigejev, Y. & Matalon, M. 2006 Nonlinear evolution of hydrodynamically unstable premixed flames. *J. Fluid Mech.* **554**, 371–392.

Sivashinsky, G. I. 1977 Diffusional-thermal theory of cellular flames. *Combust. Sci. Tech.* **15**, 137–146.

Sivashinsky, G. I. 1983 Instabilities, pattern formation, and turbulence in flames. *Annu. Rev. Fluid Mech.* **15**, 179–199.

Sivashinsky, G. I., Law, C. K. & Joulin, G. 1982 On stability of premixed flames in stagnation-point flow. *Combust. Sci. Tech.* **28**, 155–159.

Sun, C. J., Sung, C. J., He, L. & Law, C. K. 1999 Dynamics of weakly stretched flames: quantitative description and extraction of global parameters. *Combust. Flame* **118**, 108–128.

Tse, S. D., Zhu, D. L. & Law, C. K. 2000 Morphology and burning rates of expanding spherical flames in H_2/O_2/inert mixtures up to 60 atmospheres. *Proc. Combust. Inst.* **28**, 1793–1799.

Tse, S. D., Zhu, D. L. & Law, C. K. 2004 An optically accessible high-pressure combustion apparatus. *Rev. Sci. Instrum.* **75**, 233–239.

Williams, F. A. 1985 *Combustion Theory*. Benjamin-Cummins.